ACS APPLIED MATERIALS & INTERFACES

RESEARCH ARTICLE

www.acsami.org

Top-Down Process Based on Electrospinning, Twisting, and Heating for Producing One-Dimensional Carbon Nanotube Assembly

Shinji Imaizumi,[†] Hidetoshi Matsumoto,[†] Yuichi Konosu,[†] Kazuma Tsuboi,[†] Mie Minagawa,[†] Akihiko Tanioka,*[,†] Krzysztof Koziol,[‡] and Alan Windle[‡]

[†]Department of Organic and Polymeric Materials, Tokyo Institute of Technology, 2-12-1-S8-27 Ookayama, Meguro-ku, Tokyo 152-8552, Japan,

[‡]Department of Materials Science and Metallurgy, University of Cambridge, Pembroke Street, Cambridge CB2 3QZ, United Kingdom

Supporting Information

ABSTRACT: Multiwalled carbon nanotube (MWNT)/poly(vinyl butyral) (PVB) composite nanofibers were prepared by electrospinning, successive twisting and heat treatment. The MWNTs were highly oriented in an electrified thin jet during electrospinning. The heat treatment of the twisted electrospun nanofiber yarns produced the characteristics of the CNT in the composite nanofiber yarns and enhanced their electrical properties, mechanical properties, and thermal properties. The electrical conductivity of the heated yarn was significantly enhanced and showed the maximum value of 154 S cm^{-1} for the yarn heated at 400 °C. It is an order of magnitude higher than other electrospun CNT composite materials. These results demonstrated that the novel top-down process based on electrospinning, twisting, and heat treatment provide a promising option for simple and large-scale manufacture of CNT assemblies.

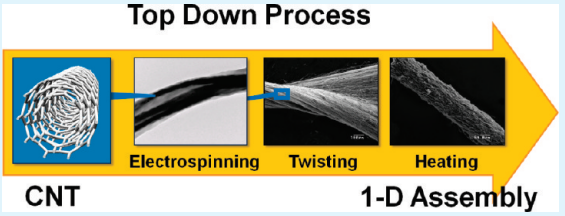

KEYWORDS: carbon nanotube, nanofiber, electrospinning, composite

INTRODUCTION

The carbon nanotube (CNT) is a promising material because of its unique structure and superior physical properties, i.e., large aspect ratio, high tensile strength (~150 GPa),[1] high Young's modulus (~ 1 TPa),[2] high electrical and thermal conductivities,[3−5] low density, and good chemical stability. However, to transfer the superior properties into practical applications, such as electronic devices, reinforcements, and biotechnology, it is necessary to find ways to process nanotubes into device structures or bulk forms. There are two main approaches, the "top-down" and "bottom-up" approaches, to fabricate the CNT assemblies. The top-down fabrication techniques from CNT dispersions have been reported; Poulin et al. drew CNT fibers by direct spinning from an aqueous CNT suspension into a poly (vinyl alcohol) solution.[6,7] Pasquali et al. processed fibers and sheets from a lyotropic liquid crystalline CNT suspension in superacids.[8,9] On the other hand, some researchers combined the spinning process with a bottom-up synthesis approach. Zhang et al. reported a "dry spinning process" to produce CNT yarns from "CNT forests" in which the CNTs were grown and vertically aligned on a substrate by chemical vapor deposition (CVD).[10,11] Windle's group developed the "direct spinning from CVD".[12] In this process, the CNT yarn is spun directly from the aerogel of CNTs formed in a CVD reactor.[13] The major advantage of the top-down approach is its straightforwardness because of utilizing commercially available CNTs without any special synthesis techniques.

This paper presents a novel top-down approach for the fabrication of nanotube assemblies by electrospinning, twisting, and heat treatment from CNT/polymer mixture solutions. Electrospinning is a simple method based on an electrohydrodynamic process for forming continuous thin fibers ranging from several nanometers to tens of micrometers.[14−16] The one-dimensional (1D) nanomaterial, CNT, can be oriented by external fields such as flow fields,[6,7,17−21] magnetic fields,[6,7,22−24] electric fields,[25,26] and electrophoretic processes.[27,28] Therefore, the CNTs are expected to be highly oriented in an electrified thin jet during electrospinning. Recently, some researchers reported that CNTs are highly oriented in the electrospun CNT/polymer composites.[29−32] However, their electrical conductivities were not very high compared to the conventional CNT fibers or yarns. We prepared aligned CNT/polymer composite nanofibers by electrospinning, then twisting them into yarns, and heating the yarns for the selective removal of the polymer component to finally form the macroscopic 1D CNT assembly.

We used a batch of multiwalled carbon nanotube (MWNT, average diameter = 50 nm) and poly (vinyl butyral) (PVB, M_w = 340 000) as the nanotube and matrix polymer, respectively. A larger diameter nanotubes are easier to suspend in polymer solution compared to thinner nanotubes (e.g., single- or double-walled nanotubes), because the attractive interaction between

Received: October 29, 2010
Accepted: January 10, 2011
Published: January 26, 2011

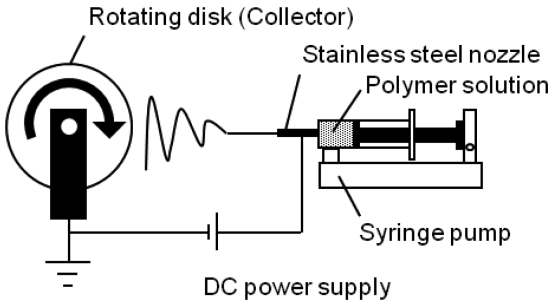

Figure 1. Schematic diagram of the apparatus used for electrospinning.

thicker tubes is lower than that between thinner tubes. In addition, we found that the MWNTs were well-dispersed in a PVB/methanol solution without using a surfactant or functionalization of the CNTs. In the present study, we first prepared highly oriented MWNT composite nanofibers using an electrohydrodynamic spinning process. Second, we removed the matrix polymer from the composite fiber yarns by heat treatment to obtain the maximum benefits from the CNTs. The aims of the present study are (i) to present novel top-down fabrication methods for CNT assemblies (MWNT yarns) by electrospinning, successive twisting, and heat treatment; and (ii) to investigate the effect of the heat treatment on the mechanical, thermal, and electrical properties of the electrospun fiber yarns.

EXPERIMENTAL SECTION

Materials. Multiwalled carbon nanotubes (MWNT-7, Lot number: 071223, average diameter = 50 nm, aspect ratio >100) were purchased from Hodogaya Chemical, Japan. Poly (vinyl butyral) (PVB) with a molecular weight of 340 000 was purchased from Wako, Japan. Methanol (MeOH) of extra-pure grade was obtained from Wako, Japan. These reagents were used without further purification. For preparation of the spinning solution, PVB was dissolved in MeOH at 8.5−10 wt %. A 0−1.5 wt % sample of the pristine MWNT was added to the polymer solution and stirred for 3 days at the stirring speed of 1 500 rpm. The solute compositions in the solutions are as follows: MWNT/PVB = 0/100, 1/99, 2/98, 5/95, 10/90, and 15/85 in wt/wt.

Electrospinning. The drawing of the electrospinning device is shown in Figure 1. The electrospinning device consists of a syringe-type infusion pump (MCIP-III, Minato Concept, Japan), and a high voltage regulated DC power supply (HAR-100P0.3, Matsusada Precision, Japan). We used a rotating disk as a collector to align the electrospun fibers (disk diameter: 250 mm, width: 5 mm). The polymer solutions were contained in a syringe with a stainless steel nozzle (0.2 mm inner diameter). The applied voltage was 15 kV; the distance between the tip of the nozzle and the collector was 100 mm; the flow rate of the solution was 0.01 mL/min; and the rotating speed of the collector was 900 rpm. The electrospinning was carried out for 1 h at 25 ± 1 °C and at less than 35% relative humidity.

Preparation of Yarn. The aligned fibers deposited on the collector were twisted to form yarns. The diameter of the prepared twisted yarns was around 350 μm. To remove the polymer matrix from the composite fiber yarns, we carried out heat treatments with the yarns in tension at 100, 200, 300, 400, and 500 °C in a ceramic furnace for 2 h under a continuous nitrogen purge.

Characterization and Instruments. The surface morphologies of the prepared nanofibers and nanofiber yarns were observed using a scanning electron microscope (SEM, SM-200, Topcon, Japan) operated at 10 kV. All SEM samples were sputter-coated with Au. The internal structure of the prepared nanofiber was evaluated using a transmission electron microscope (TEM, H-7650, Hitachi, Japan) operated at 100 kV and a 3D Raman microscopy system (Nanofinder 30, Tokyo Instruments, Japan). The polarized Raman spectra, generated by excitation with 514.5 nm radiation from an argon ion laser (Innova300, COHERENT) were obtained with a 100 s integration time. The irradiated power of the excitation beam was about 20 mW at the sample surface. The polarization of the excitation beam was controlled with a half wave plate. The pyrolytic behavior of the pristine PVB nanofiber yarn and the MWNT/PVB (10/90) composite nanofiber yarn in N_2 was investigated by thermogravimetric-differential thermal analysis (TG-DTA) using an analyzer (TG8120, Rigaku, Japan). The electrical conductivity of the prepared yarn was measured using the DC two-probe method. The electrodes were fixed to both ends of the yarns with silver paste. The distance between the electrodes was 20 mm. Five samples were tested for each yarn. The linear density (LD) and specific gravity (SG) of the prepared yarns were calculated by the following equations

$$(LD) = m/L \tag{1}$$

$$(SG) = m/(SL\rho_W) \tag{2}$$

where m is the mass, L is the length, S is the cross-section area, and ρ_W is the density of water. The mass of the prepared yarns were measured using a nanobalance (Sartorius, Germany). The mechanical properties of the prepared yarns were measured by a dedicated fiber tester (Favimat, Textechno, Germany). The gauge length of the initial sample was 20 mm, and the strain rate was 2 mm/min. Ten samples were tested for each yarn. The thermal conductivity κ is expressed by the following equation

$$\kappa = \rho D c \tag{3}$$

where ρ is the specimen density ($SG \times \rho_W$), D is the thermal diffusivity, and c is the specific heat of the sample. To measure D, we use Angstrom's method, which is a highly accurate method for determining D of a long and thin rod.[33,34] This method employs a long, thin radiating rod with a heat source whose temperature sinusoidally varies with time at one end (see Figure 2a). In this system, the thermal diffusivity D is expressed by the following equation[34,35]

$$D = \frac{l^2}{2(\Delta t)\ln(T_1/T_2)} \tag{4}$$

where l is the distance between two thermocouples, T_1 and T_2 are the amplitude of the thermal waves, and Δt is the time delay (the time taken by the thermal wave to travel from one sensor to the other). The temperature response of the heated composite yarn was recorded by a thermal camera (FLIR ThermaCAM SC3000) at the different measuring points (see Figure 2b). Samples were connected to the heat source, a resistively heated strain gauge. Sinusoidal heat waves of peak-to-peak amplitude (10 V) were passed through specimens at a frequency of 5 mHz. Ten samples were tested for each yarn. Specific heat capacities of the samples were measured by modulated DSC. The measurements were performed on a TA Instrument DSC Q2000.

RESULTS AND DISCUSSION

Preparation and Characterization of Highly Oriented Nanotube Composite Nanofibers by Electrospinning. We succeeded in preparing homogeneous (bead-free) fibers from spinning solutions (MWNT/PVB = 0/100, 1/99, 2/98, 5/95 and 10/90 in wt/wt) with a good spinnability to form aligned fibers using a rotating disk as the collector (effect of MWNT content on morphology of the as-spun fiber is shown in Figure S1 in the Supporting Information). Figure 3a−e shows the aligned MWNT/PVB fibers. Their diameters are around 400 nm and their morphologies were smooth. The yarns were prepared by

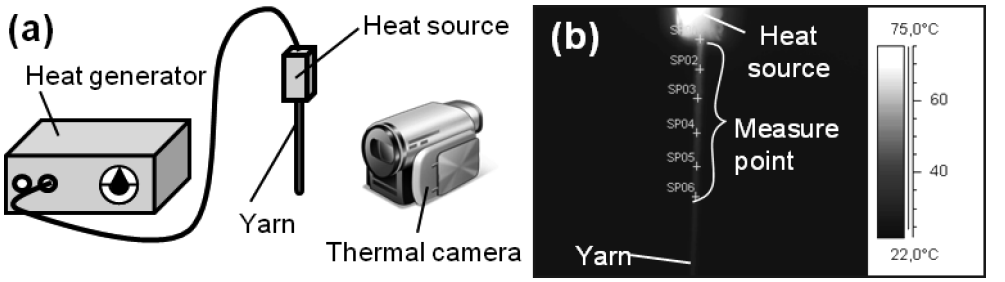

Figure 2. (a) Schematic diagram of Angstrom's apparatus to measure the thermal diffusivity and (b) the thermal image of the MWNT/PVB composite yarns taken by a thermal camera.

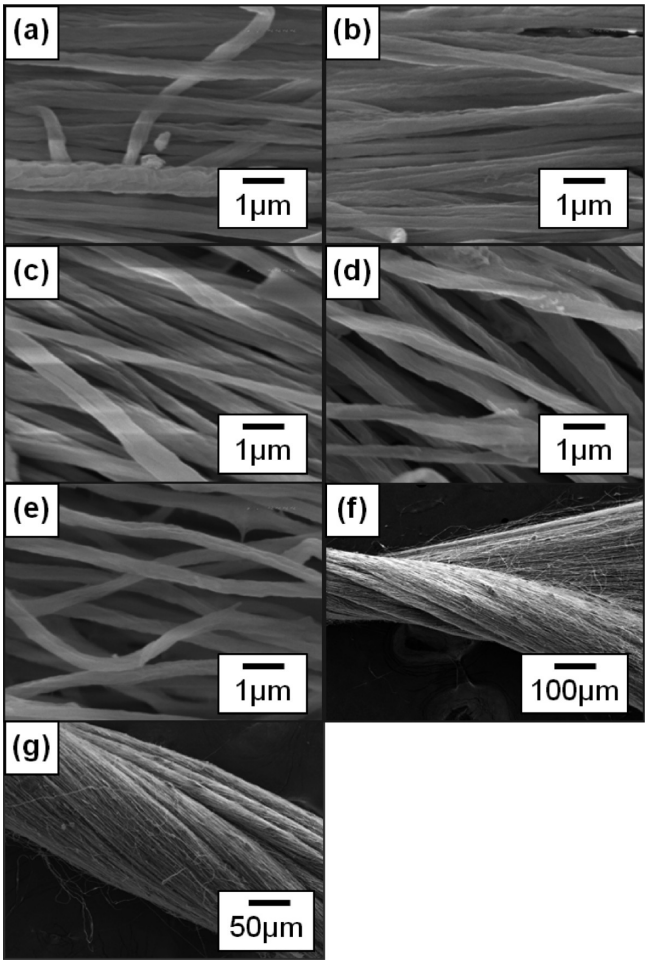

Figure 3. Surface SEM images of the PVB/MWNT composite nanofibers: (a) PVB nanofiber; composite nanofibers containing (b)1 wt % MWNT, (c) 2 wt % MWNT, (d) 5 wt % MWNT, and (e) 10 wt % MWNT; (f, g) twisted nanofiber yarn of e.

twisting of the aligned nanofibers (see Figure 3f). The twist count was approximately 500 turns per meter (calculated from the SEM image shown in Figure 3g) and the diameter of the yarns was approximately 350 μm.

Figure 4 shows the polarized Raman spectra of the MWNT/PVB composite fiber (MWNT/PVB = 10/90). The typical peaks are a small D-band around 1360 cm^{-1} corresponding to the amorphous carbon and structural defects (A_{1g}) and a large G-band around 1580 cm^{-1} corresponding to the graphite structures and tangential shearing mode of the carbon atom

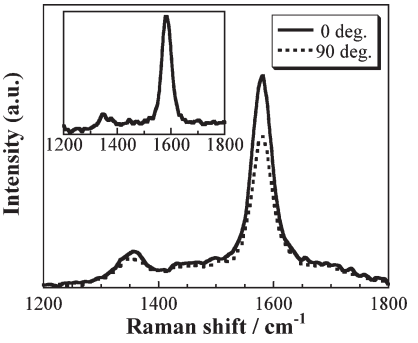

Figure 4. Polarized Raman spectra of the MWNT/PVB composite fiber (10wt.% MWNT). The insert is that of the pristine MWNT.

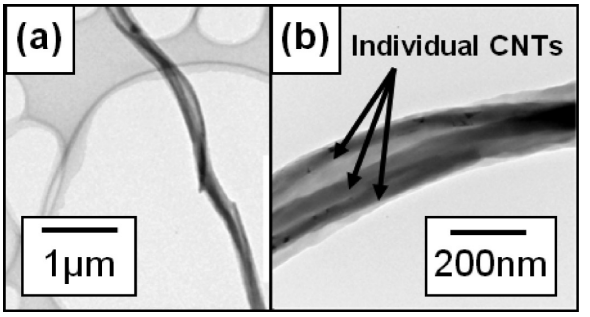

Figure 5. Typical TEM images of the as-spun MWNT/PVB composite nanofiber (10 wt % MWNT): (a) low-magnification image and (b) high-magnification image.

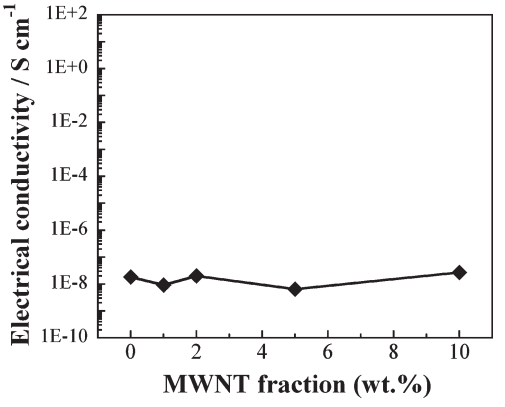

Figure 6. Electrical conductivity of the MWNT/PVB composite fiber yarn as a function of the MWNT content.

Table 1. Effect of MWNT Content on Properties of MWNT/PVB Composite Fiber Yarns

no.	CNT content (wt %)	linear density (tex (= g km^{-1}))	elongation (%)	specific strength (N tex^{-1} (= GPa SG^{-1}))	specific stiffness (N tex^{-1} (= GPa SG^{-1}))
1	0	38.8	61.81 ± 4.68	0.057 ± 0.001	0.70 ± 0.13
2	1	33.5	32.63 ± 9.55	0.058 ± 0.001	0.81 ± 0.11
3	2	30.1	30.50 ± 9.35	0.069 ± 0.002	0.83 ± 0.10
4	5	26.7	24.4 ± 8.61	0.053 ± 0.001	0.95 ± 0.13
5	10	24.7	19.2 ± 3.21	0.045 ± 0.001	1.10 ± 0.18

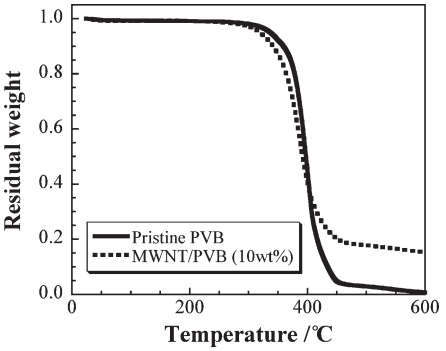

Figure 7. Thermogravimetric curves for the MWNT/PVB composite fiber yarns (0 and 10 wt % MWNT).

(E_{2g}). These obtained peaks are identical with the peaks in Raman spectrum of pristine MWNT (Figure 4 inset[36−38]). This serves as a direct confirmation of the successful filling of the MWNTs in the as-spun fiber. The intensity ratio of G-band between the spectra for the different polarized-angle 0° (parallel to fiber axis) and 90° (vertical to axis) (the more detailed polarization dependence of G-band intensity of Raman spectra is shown in Figure S2 in the Supporting Information), $I_G(0°)$: $I_G(90°)$ = 1.00: 0.67 agrees with Rao's experimental result for the aligned MWNTs vertically grown on a quartz substrate, $I_G(0°)$: $I_G(90°)$ = 1.00:0.57.[39] This supports the fact that the MWNTs in the composite fiber are aligned nearly parallel to the fiber axis. A TEM analysis was carried out to characterize the orientation of the MWNTs in the composite fiber (MWNT/PVB = 10/90). The TEM images showed that the MWNTs were highly oriented parallel to the fiber axis of the fibers (Figure 5) as expected. The orientation of the MWNTs was due to the electrified liquid flow formed during electrospinning as reported in previous studies.[29−32]

Figure 6 shows the additive effect of the MWNT on the electrical conductivity of the as-spun composite fiber. The electrical conductivity for the all yarns was around 10^{-8} S/cm. This result indicates that the matrix polymer blocks the electrical contacts between the nanotubes. The effect of the MWNT content on the mechanical properties of the MWNT/PVB composite fiber yarns is summarized in Table 1 (stress−strain curves were included in the Supporting Information, see Figure S3). It can be seen that the yarn's elongation decreased from 61 to 19% with an increase in the MWNT content in the fiber. The addition of the MWNTs improved the specific stiffness (Young's modulus) of the yarn from 0.70 to 1.10 N tex^{-1} with an increase in the MWNT content in the fiber. The decrease in the elongation and the increase in the specific stiffness indicate that the rigid MWNTs dispersed in the nanofiber hinder the movement of polymer chains and enhanced the stiffness of the composite

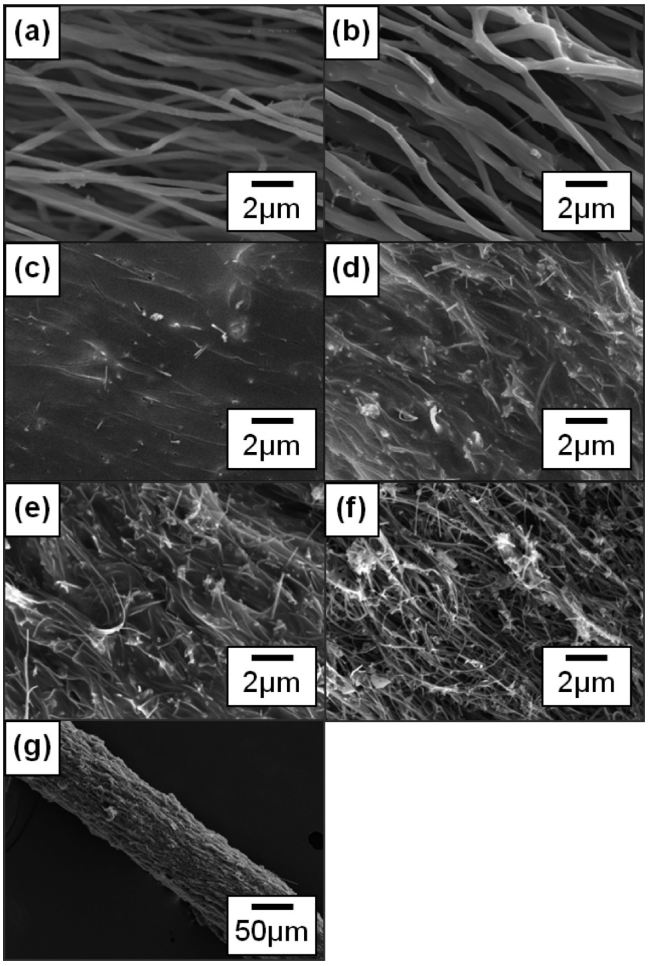

Figure 8. Surface SEM images of the MWNT/PVB composite fiber yarns (10 wt % MWNT) heated in N_2 at various temperatures for 2 h: (a) 0, (b) 100, (c) 200, (d) 300, (e) 400, and (f) 500; (g) low-magnification image of f.

nanofiber yarn. On the other hand, the specific tensile strength showed a peak at 2 wt % (0.069 N tex^{-1}). The decrease in the tensile strength of the samples above 2 wt % MWNT may be caused by the nonhomogeneous filling of the MWNTs during nanofiber preparation in the higher CNT-composite nanofibers, which was supported by the TEM image (see Figure 5a).

Effects of Heat Treatment on the Yarns. As described in the previous section, the contribution of the matrix polymer to the physical properties of the composites was substantial. Therefore, an approach to produce the characteristics of nanotubes in the composites was strongly required. To reduce the effect of the PVB in the composites, the yarns were heat-treated at 100, 200,

Table 2. Effect of Heat Temperature on Properties of MWNT/PVB Composite Fiber Yarns

no.	heat temperature (°C)	linear density (tex (= g km^{-1})	specific gravity (SG)	elongation (%)	specific strength (N tex^{-1} (= GPa SG^{-1}))	specific stiffness (N tex^{-1} (= GPa SG^{-1}))
1	as-spun	24.7	0.09	19.19 ± 3.21	0.045 ± 0.006	1.10 ± 0.18
2	100	17.3	0.65	89.9 ± 5.99	0.065 ± 0.009	3.30 ± 0.15
3	200	16.2	1.45	44.41 ± 2.36	0.066 ± 0.006	4.45 ± 0.62
4	300	16.1	1.88	2.23 ± 0.26	0.076 ± 0.005	4.70 ± 0.33
5	400	5.01	0.47	0.38 ± 0.05	0.027 ± 0.003	7.40 ± 0.59
6	500	4.15	0.42	0.47 ± 0.04	0.047 ± 0.003	11.94 ± 0.91

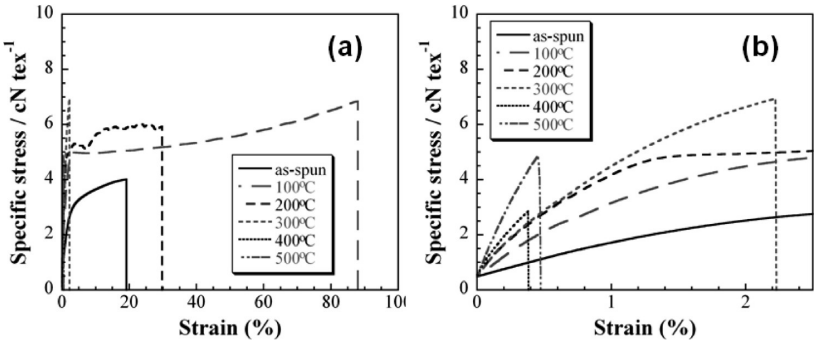

Figure 9. (a) Typical specific stress−strain curves for the heated MWNT/PVB composite fiber yarn. Heat temperature: 0 (as-spun), 100, 200, 300, 400, and 500 °C. These curves are as-recorded, and the gauge length was 20 mm for all the samples. (b) magnifies the region of small strain.

300, 400, and 500 °C for 2 h in a nitrogen atmosphere. Figure 7 shows the thermogravimetric curves for the pristine PVB fiber yarn and the MWNT/PVB composite fiber yarn. For the pristine PVB fiber yarn, the decomposition started at 295 °C and finished at around 500 °C and 2.9 wt % of the residues remained. For the composite fiber yarn (MWNT/PVB = 10/90), on the other hand, the PVB decomposition began at 290 °C and ended around 500 °C, but 8.6 wt % of the residues remained (the MWNT content in the yarn was increased to approximately 56 wt % at 500 °C). The FT-IR spectra of the as-spun and heated MWNT/PVB composite fiber yarns are shown in Figure S4 in the Supporting Information. From the FT-IR spectra, we can confirm that the peaks of the matrix material changed at 300 °C and disappeared at 400 °C (more detailed discussion is included in the Supporting Information). This result indicates that most of the PVB is thermally decomposed above 400 °C, but the development of cyclic and cross-linked compounds of hydrocarbon residues leads to the formation of carbonaceous residues.[40] The carbon residues function as a binder between the nanotubes and maintain the formation of the yarns. Figure 8 shows the surface SEM images of the heated composite fiber yarn (MWNT/PVB = 10/90). Above 200 °C, the composite nanofibers adhered to each other, and above 300 °C, more MWNTs appeared at the surface of the yarns, but the formation of the yarn was maintained.

The effect of the temperature on the densities of the composite fiber yarns is summarized in Table 2. The linear density of the heated yarns gradually decreased with an increase in the heating temperature. It significantly decreased at 0−100 and 300−400 °C. This was caused by evaporation of the remaining solvent (MeOH) in the fiber around 64.5 °C (T_b of MeOH) and the thermal decomposition of PVB above 300 °C (see Figure 7 and Figure S4 in the Supporting Information). The behavior of the matrix material at higher temperatures is obviously characterized by the SG which showed a peak at 300 °C. This was caused by the densification of the yarn due to the rearrangement of the polymer chain above approximately 75 °C (T_g of PVB), the melting of the polymer around 200 °C, and the thermal decomposition of PVB above 300 °C. We can find the densification of the yarn heated at 300 °C by comparing Figure 8g with Figure 3g. The stress−strain ($S-S$) curves of the heated fibers are shown in Figure 9 and the mechanical properties are listed in Table 2. As can be seen in the $S-S$ curves, elongation of the yarns reached the highest value at the heat treatment temperature of 100 °C, and then it tends to decrease with an increase in the temperature. In addition, specific stiffness (obtained from the initial slope of the $S-S$ curves in Figure 9b) increased from 1.1 to 11.9 N tex^{-1} with an increase in the temperature (see Table 2). These mechanical properties of the heated composite yarns were mainly determined by the thermal behaviors of the polymer matrix (i.e., densification around 100 °C, melting around 200 °C, and thermal decomposition above 300 °C). The specific strength reached the highest value of 0.076 N tex^{-1} (approximately 143 MPa) at 300 °C, and then it decreased with an increase in the temperature. The decrease in the specific strength above 300 °C was due to the thermal decomposition of the polymer (see Figure 7 and Figure S4 in the Supporting Information).

The thermal diffusivity and thermal conductivity of the heated yarn are shown in Figure 10. To calculate the thermal conductivity, we used specific heat value of 4.50 J g^{-1} K^{-1}, obtained by our DSC measurements. The thermal diffusivity of the heated yarn was improved from 1.12 to 2.96 mm^2 s^{-1} by increasing the temperature. It indicates that phonons can more easily transfer between the carbon nanotubes in the absence of the scattering polymer matrix because of the decomposition of the polymer. The heat conductivity of the yarn showed a peak at 300 °C. The decrease in the thermal conductivity above 300 °C was influenced by a decrease in the specimen density of the yarn ($SG\rho_W$)

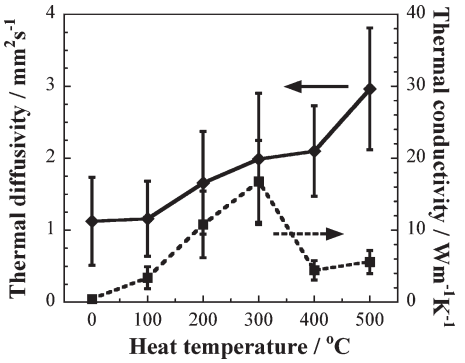

Figure 10. The thermal diffusivity and thermal conductivity of the MWNT/PVB composite fiber yarn as a function of the heat-treatment temperature on the 10 wt % MWNT loaded yarn.

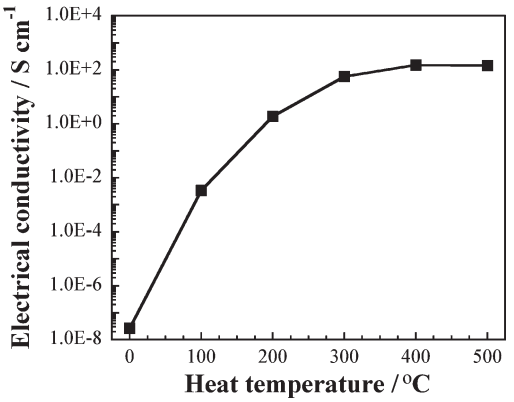

Figure 11. Electrical conductivity of the MWNT/PVB composite fiber yarn (10 wt % MWNT) as a function of the heat-treatment temperature.

because of the thermal decomposition of the polymer (see Table 2, Figure 7, and Figure S4 in the Supporting Information). To enhance the thermal conductivity, some treatments for the densification of the heated yarn will be required. The best thermal conductivity value of the composite yarn heated at 300 °C was 16.8 W m^{-1} K^{-1}.

Figure 11 shows the effect of the heat-treatment temperature on the electrical conductivity of the MWNT/PVB composite yarn. The high-temperature treatment significantly improved the conductivity. This is due to an increase in the interfacial contact between the nanotubes caused by decomposition of the PVB. The conductivity was saturated above 400 °C, where most of the PVB in the yarn was decomposed (see Figures 7 and Figure S4 in the Supporting Information). The maximum conductivity was 154 ± 9.6 S cm^{-1}. This value was an order of magnitude higher than that of the reported electrospun CNT composite materials (the best value was ~35 S cm^{-1} for the MWNT-composite carbon fibers[41]), and as high as that of the SWNT/polymer fiber prepared by the other top-down approach (140 S cm^{-1}).[7] However, at present, the conductivity of the electrospun CNT composite materials are low compared to that prepared by the bottom-up approach (~8000 S cm^{-1} for single-walled CNT yarns[12]). To accomplish complete transfer of the superior CNT properties into the electrospun yarns, further optimization of the top-down approach to enhance the interaction between the CNTs should be required (e.g., utilizing of highly concentrates CNT-dispersed spinning solution, and densification of the specimen during the heat treatment).

CONCLUSION

In the present study, MWNT yarns were prepared by electrospinning, twisting, and heat treatment. The TEM analysis showed that the MWNTs are highly oriented along the fiber axis in the prepared composite fibers. This is due to the electrified liquid jet formed by the electrohydrodynamic spinning process. While the addition of the MWNTs improved the mechanical properties of the composite fiber yarns, the electrical conductivity of the yarns was determined by the matrix polymer. The heat treatment determined the characteristics of the CNT out of the composite nanofiber yarns and enhanced their mechanical, thermal, and electrical properties. In particular, the electrical conductivity of the heated yarn was significantly enhanced. The maximum value was 154 S cm^{-1}, which was an order of magnitude higher than that of the other electrospun CNT composite materials. These results demonstrated that the combination of electrospinning, twisting, and heat treatment provide a promising option for simple and large-scale producing CNT assemblies. The 1D CNT assembly is potentially applicable to the high-performance materials such as electrodes for fuel cells, secondary batteries, and capacitors, lightweight heat sinks, and reinforcements for lightweight composites. At present, we have not accomplished the complete transfer of the nanoscopic CNT properties into the macroscopic 1D assembly through our top-down approach. It is concluded that the physical properties of the yarns will be improved by optimization of some parameters (e.g., spinning solutions with higher content of dispersed nanotubes including higher-aspect-ratio nanotubes; and densification of the specimen during the heat treatment). Further studies are now in progress and the results will be reported.

ASSOCIATED CONTENT

Supporting Information. Surface SEM images of the as-spun MWNT/PVB composite nanofibers, polarization dependence of Raman spectra of the as-spun MWNT/PVB composite nanofibers, specific stress−strain curves for the as-spun MWNT/PVB composite fiber yarns, and FT-IR spectra of the as-spun and heated MWNT/PVB composite fiber yarns (PDF). This material is available free of charge via the Internet at http://pubs.acs.org.

AUTHOR INFORMATION

Corresponding Author

*Phone: +81-3-5734-2426. Fax: +81-3-5734-2876. E-mail: tanioka.a.aa@m.titech.ac.jp.

REFERENCES

(1) Treacy, M.; Ebbesen, T. W.; Gibson, J. M. *Nature* **1996**, *381*, 678–680.

(2) Yu, M.; Lourie, O.; Dyer, M. J.; Kelly, T. F.; Ruoff, R. S. *Science* **2000**, *287*, 637–640.

(3) Wei, B. Q.; Vajtai, R.; Ajayan, P. M. *Appl. Phys. Lett.* **2001**, *79*, 1172–1174.

(4) Fischer, J. E.; Zhou, W.; Vavro, J.; Llaguno, M. C.; Guthy, C.; Haggenmueller, R. *J. Appl. Phys.* **2003**, *93*, 2157–2163.

(5) Kim, P.; Shi, L.; Majumdar, A.; McEuen, P. L. *Phys. Rev. Lett.* **2001**, *87*, 215502/1–215502/4.

(6) Vigolo, B.; Penicaud, A.; Coulon, C.; Sauder, C.; Pailler, R.; Journet, C.; Bernier, P.; Poulin, P. *Science* **2000**, *290*, 1331–1334.
(7) Kozlov, M. E.; Capps, R. C.; Sampson, W. M.; Ebron, V. H.; Ferraris, J. P.; Baughman, R. H. *Adv. Mater.* **2005**, *17*, 614–617.
(8) Zhou, W.; Vavro, J.; Guthy, C.; Winey, K. I.; Fischer, J. E.; Ericson, L. M.; Ramesh, S.; Saini, R.; Davis, V. A.; Kittrell, C.; Pasquali, M.; Hauge, R. H.; Smalley, R. E. *J. Appl. Phys.* **2004**, *95*, 649–655.
(9) Ericson, L. M.; Fan, H.; Peng, H.; Davis, V. A.; Zhou, W.; Sulpizio, J.; Wang, Y.; Booker, R.; Vavro, J.; Guthy, C.; Parra-Vasquez, A. N. G.; Kim, M. J.; Ramesh, S.; Saini, R. K.; Kittrell, C.; Lavin, G.; Schmidt, H.; Adam, W. W.; Billups, W. E.; Pasquali, M.; Hwang, W. F.; Hauge, R. H.; Fisher, J. E.; Smalley, R. E. *Science* **2004**, *305*, 1447–1450.
(10) Zhang, M.; Atkinson, K. R.; Baughman, R. H. *Science* **2004**, *306*, 1358–1361.
(11) Zhang, M.; Fang, S.; Zakhidov, A. A.; Lee, S. B.; Aliev, A. E.; Williams, C. D.; Atkinson, K. R.; Baughman, R. H. *Science* **2005**, *309*, 1215–1219.
(12) Li, Y. L.; Kinloch, I. A.; Windle, A. H. *Science* **2004**, *304*, 276–278.
(13) Koziol, K.; Vilatela, J.; Moisala, A.; Motta, M.; Cunniff, P.; Sennett, M.; Windle, A. *Science* **2007**, *318*, 1892–1895.
(14) Doshi, J.; Reneker, D. H. *J. Electrostat.* **1995**, *35*, 151–160.
(15) Reneker, D. H.; Chun, I. *Nanotechnology* **1996**, *7*, 216–223.
(16) Yarin, A. L.; Koombhongse, S.; Reneker, D. H. *J. Appl. Phys.* **2001**, *90*, 4836–4846.
(17) Hobbie, E. K.; Wang, H.; Kim, H.; Lin-Gibson, S.; Grulke, E. A. *Phys. Fluids* **2003**, *15*, 1196–1202.
(18) Lay, M. D.; Novak, J. P.; Snow, E. S. *Nano Lett.* **2004**, *4*, 603–606.
(19) Xin, H.; Woolley, A. T. *Nano Lett.* **2004**, *4*, 1481–1484.
(20) Chen, Y.; Yu, J. *Carbon* **2005**, *43*, 3183–3186.
(21) Liu, Y.-T.; Xie, X.-M.; Gao, Y.-F.; Feng, Q.-P.; Guo, L.-R.; Wang, X.-H.; Ye, X.-Y. *Mater. Lett.* **2007**, *61*, 334–338.
(22) Smith, B. W.; Benes, Z.; Luzzi, D. E.; Fischer, J. E.; Walters, D. A.; Casavant, M. J.; Schmidt, J.; Smalley, R. E. *Appl. Phys. Lett.* **2000**, *77*, 663–665.
(23) Hone, J.; Llaguno, M. C.; Nemes, N. M.; Jonson, A. T.; Fischer, J. E.; Walters, D. A.; Casavant, M. J.; Schmidt, J.; Smalley, R. E. *Appl. Phys. Lett.* **2000**, *77*, 666–668.
(24) Walters, D. A.; Casavant, M. J.; Qin, X. C.; Huffman, C. B.; Boul, P. J.; Ericson, L. M. *Chem. Phys. Lett.* **2001**, *338*, 14–20.
(25) Chen, X. Q.; Saito, T.; Yamada, H.; Matsushige, K. *Appl. Phys. Lett.* **2001**, *78*, 3714–3716.
(26) Diehl, M. R.; Yaliraki, S. N.; Beckman, R. A.; Barahona, M.; Heath, J. R. *Angew. Chem., Int. Ed.* **2002**, *41*, 353–356.
(27) Gommans, H. H.; Alldredge, J. W.; Tashiro, H.; Park, J.; Magnuson, J.; Rinzler, A. G. *J. Appl. Phys.* **2000**, *88*, 2509–2514.
(28) Hwang, J.; Gommans, H. H.; Ugawa, A.; Tashiro, H.; Haggenmueller, R.; Winey, K. I.; Fischer, J. E.; Tanner, D. B.; Rinzler, A. G. *Phys. Rev. B.* **2000**, *62*, R13310–R13313.
(29) Hou, H.; Ge, J. J.; Zheng, J.; Li, Q.; Reneker, D. H.; Greiner, A.; Cheng, S. Z. D. *Chem. Mater.* **2005**, *17*, 967–973.
(30) Ra, E. J.; An, K. H.; Kim, K. K.; Jeong, S. Y.; Lee, Y. H. *Chem. Phys. Lett.* **2005**, *413*, 188–193.
(31) Sundaray, B.; Subramanian, V.; Natarajan, T. S.; Krishnamurthy, K. *Appl. Phys. Lett.* **2006**, *88*, 143114/1–143114/3.
(32) Wang, G.; Tan, Z.; Liu, X.; Chawda, S.; Koo1, J. S.; Samuilov, V.; Dudley, M. *Nanotechnology* **2006**, *17*, 5829–5835.
(33) Angstrom, A. J. *Ann. Chim. Phys.* **1861**, *144*, 513.
(34) Prociak, A.; Sterzynski, T.; Pielichowski *J. Polym. Eng. Sci.* **1999**, *39*, 1689–1695.
(35) Belling, J. M.; Unsworth, J. *Rev. Sci. Instrum.* **1987**, *58*, 997–1002.
(36) Eklund, P. C.; Holden, J. M.; Jishi, R. A. *Carbon* **1995**, *33*, 959–972.
(37) Holden, J. M.; Zhou, P.; Bi, X. X.; Eklund, P. C.; Bandow, S.; Jishi, R. A.; Chowdhury, K. D.; Dresselhaus, G.; Dresselhaus, M. S. *Chem. Phys. Lett.* **1994**, *220*, 186–191.
(38) Hwang, J.; Gommans, H. H.; Ugawa, A.; Tashiro, H.; Haggenmueller, R.; Winey, K. I.; Fischer, J. E.; Tanner, D. B.; Rinzler, A. G. *Phys. Rev. B.* **2000**, *62*, R13310–R13313.
(39) Rao, A. M.; Jorio, J.; Pimenta, M. A.; Dantas, M. S. S.; Dresselhaus, G.; Dresselhaus, M. S. *Phys. Rev. Lett.* **2000**, *84*, 1820–1823. Rao et al. reported that the polarized Raman spectra of the aligned MWNTs depended on the polarization of both excitation beam and emitted Raman signals, whereas we measured the polarization dependence of the excitation beam. They reported the value of XX:YY:XY:YX = 1.00:0.29:0.19:0.39, where X and Y indicate polarization directions parallel and normal to long axis of MWNTs, respectively, and the former letter indicates polarization of excitation beam and the latter indicates that of emitted Raman signal. We evaluated their value of $I_G(0°):I_G(90°)$ corresponding to (XX+XY:YY+YX) = 1.00:0.57.
(40) Salam, L. A; Matthews, R. D; Robertson, H. *J. Eur. Ceram. Soc.* **2000**, *20*, 1375–2383.
(41) Ra, E. J.; An, K. H.; Kim, K. K.; Jeong, S. Y.; Lee, Y. H. *Chem. Phys. Lett.* **2005**, *413*, 188–193.